JGR Solid Earth

RESEARCH ARTICLE
10.1029/2022JB024863

Imaging the Volcanic Structures Beneath Gran Canaria Island Using New Gravity Data

F. G. Montesinos[1,2], J. Arnoso[2,3], D. Gómez-Ortiz[4], M. Benavent[1,2], I. Blanco-Montenegro[2,5], E. Vélez[2,3], T. Martín-Crespo[4], A. V. Gorbatikov[6], and M. Y. Stepanova[6]

[1]Facultad de CC. Matemáticas, Universidad Complutense de Madrid, Madrid, Spain, [2]Research Group 'Geodesia', Universidad Complutense de Madrid, Madrid, Spain, [3]Instituto de Geociencias (IGEO), Madrid, Spain, [4]Dpt. Biología y Geología, Física y Química Inorgánica, ESCET, Universidad Rey Juan Carlos, Madrid, Spain, [5]Departamento de Física, Escuela Politécnica Superior, Universidad de Burgos, Burgos, Spain, [6]Institute of Physics of the Earth, Russian Academy of Sciences, Moscow, Russia

Key Points:

- We have obtained a gravity anomaly map for Gran Canaria from a new data set, which was inverted to model the shallow subsurface structures
- The interpretation of the gravity model improves our knowledge about subsurface structures and the volcanic evolution of this island

Supporting Information:

Supporting Information may be found in the online version of this article.

Correspondence to:

F. G. Montesinos,
fuensant@ucm.es

Citation:

Montesinos, F. G., Arnoso, J., Gómez-Ortiz, D., Benavent, M., Blanco-Montenegro, I., Vélez, E., et al. (2022). Imaging the volcanic structures beneath Gran Canaria Island using new gravity data. *Journal of Geophysical Research: Solid Earth*, *127*, e2022JB024863. https://doi.org/10.1029/2022JB024863

Received 30 MAY 2022
Accepted 17 OCT 2022

Author Contributions:

Conceptualization: F. G. Montesinos, J. Arnoso, D. Gómez-Ortiz, A. V. Gorbatikov
Data curation: F. G. Montesinos, M. Benavent, E. Vélez
Formal analysis: F. G. Montesinos, J. Arnoso, D. Gómez-Ortiz, M. Benavent, I. Blanco-Montenegro, E. Vélez, T. Martín-Crespo, A. V. Gorbatikov, M. Y. Stepanova
Investigation: F. G. Montesinos, J. Arnoso, D. Gómez-Ortiz, M. Benavent, I. Blanco-Montenegro, E. Vélez, T. Martín-Crespo, A. V. Gorbatikov
Methodology: F. G. Montesinos

Abstract From a new gravity data set that covers homogeneously the whole surface of Gran Canaria (Canary Islands, Spain) and marine gravity data in the nearest offshore, we have obtained a Bouguer anomaly gravity map of the island which improves the previous ones. Using these gravity anomalies, we have applied a gravity inversion approach to investigate the structures beneath the surface of Gran Canaria Island and derive a 3D gravity sources model. The geometry of structures with anomalous density values is constrained up to a depth of approximately 20,000 m below the sea level. The interpretation of the density model identified structures related to the different volcanic stages of Gran Canaria. Several deep-rooted high-density structures represent the intrusive bodies emplaced in the early formation of Gran Canaria and the magma plumbing system of the Miocene volcanic edifices. A low-density body in the center of the island may be associated with the syenitic core of the felsic central volcanic edifice (Tejeda Caldera). Shallow low-density structures identified fractures which acted as feeder dikes of monogenetic volcanoes during the rejuvenated stage. Finally, the NW-SE rift, which is the most important volcano-tectonic structure of Gran Canaria, has a characteristic gravimetric signature and represents a long-lived extensional fracture zone that has controlled the volcanic activity at least since the Miocene.

Plain Language Summary We present a study of Gran Canaria Island (Canarian Archipelago, Spain) that provides a new model of the sources of the gravity field through the inversion of a new land and marine gravity data set. This model identifies several high-density crustal structures that correspond to the intrusive bodies emplaced in the early formation of Gran Canaria. A low-density body revealed in the center of the island is associated with the central volcanic edifice, the Tejeda Caldera. Other structures unveiled in the model are related to different volcanic stages and volcano-tectonic features of Gran Canaria Island.

1. Introduction

Gran Canaria is one of the seven major islands of the Canary Archipelago (Spain), which is a volcanic chain located in the Atlantic Ocean (latitude: 27–29°N, longitude: 13–18°W) (Figure 1). The building of this archipelago was related to the opening of the Atlantic and several hypotheses about its genesis have been proposed: the hot spot hypothesis (Hoernle & Schmincke, 1993); a propagating fracture from the Atlas Mountains (Anguita & Hernán, 1975); and mantle decompression melting together with the uplift of tectonic blocks (Araña & Ortiz, 1991). After the unifying theory of Anguita and Hernán (2000), recent studies (Blanco-Montenegro et al., 2018) have shown that regional crustal tectonics are key to explaining the pathways followed by the magma toward the surface to build the Canary volcanic edifices.

The subaerial eruptive activity in Gran Canaria started about 14.5 My ago and consisted of several volcanic stages including the building of a shield volcano and a later rejuvenated stage after a long erosional gap (e.g., Carracedo, 1999; Carracedo et al., 2002; McDougall & Schmincke, 1976). The volume of the subaerial portion of the island was estimated as approximately 850 km^3 by Schmincke and Sumita (1998) and Funck and Schmincke (1998), which represents 2.0%–2.3% of the volcanic edifice, whereas the volume of the submarine edifice of Gran Canaria and its apron was estimated at >24,000 km^3. This means that the stage of submarine volcanism in Gran Canaria represents more than 90% of the total island volume (e.g., Krastel & Schmincke, 2002;

Project Administration: J. Arnoso
Resources: F. G. Montesinos, J. Arnoso, I. Blanco-Montenegro
Software: F. G. Montesinos
Supervision: F. G. Montesinos, J. Arnoso, D. Gómez-Ortiz, I. Blanco-Montenegro, T. Martín-Crespo
Validation: F. G. Montesinos, I. Blanco-Montenegro
Visualization: F. G. Montesinos, D. Gómez-Ortiz
Writing – original draft: F. G. Montesinos, J. Arnoso, D. Gómez-Ortiz, M. Benavent, I. Blanco-Montenegro, E. Vélez, T. Martín-Crespo, A. V. Gorbatikov, M. Y. Stepanova
Writing – review & editing: F. G. Montesinos, J. Arnoso, D. Gómez-Ortiz, M. Benavent, I. Blanco-Montenegro, E. Vélez, T. Martín-Crespo, A. V. Gorbatikov, M. Y. Stepanova

McDougall & Schmincke, 1976), although it has not been studied to a great extent. The age, structure and volume of the submarine edifice are almost unknown due to the absence of subaerial outcrops of its materials, but they can be inferred from bathymetric and geophysical data. For this reason, the use of geophysical techniques is essential to gather a better knowledge of the volcanic history of the island by modeling the crustal structures from shallow to deep levels.

We present here the results obtained from a gravity inversion approach applied to investigate the structures beneath the surface of Gran Canaria Island.

Some previous gravity studies modeled the inner structure of Gran Canaria (Bosshard & MacFarlane, 1970; Camacho et al., 2000). However, these authors interpreted the gravity map of the island using a scarce land data set, having large areas without information. Other potential field studies were achieved by analysis and forward modeling of the aeromagnetic anomaly map of this island (Blanco-Montenegro et al., 2003). From an inversion approach of aeromagnetic data, Blanco-Montenegro et al. (2018) studied a magnetic anomaly detected over the NW submarine portion of the volcanic edifice, revealing a large, reversely magnetized, elongated structure with ENE-WSE orientation. This body was interpreted as a magmatic intrusion ascribed to the submarine stage of growth of Gran Canaria. Recently, Ledo et al. (2021) obtained a 3D electrical resistivity model from a new magnetotelluric data set. This model identifies high and low resistivity values, which are explained by the presence of highly porous materials and fractures and hydrothermal alteration or convective cells, respectively.

Other constraints were derived from seismic data measured in offshore areas (Funck et al., 1996; Ye et al., 1999). Funck et al. (1996) published a study about the seismic structure of the volcanic apron north of Gran Canaria. Through wide-angle reflection data and refraction data across three radial profiles, Ye et al. (1999) studied the inner structure of the island and the adjacent basin. The submarine stage of Gran Canaria has been also studied by the Ocean Drilling Program (e.g., Schmincke & Segschneider, 1998; Schmincke & Sumita, 1998; Schmincke et al., 1995).

There are many gravimetric studies in volcanic areas (e.g., Fedi et al., 2018; Montesinos et al., 2006, 2011; Sainz-Maza Aparicio et al., 2019), which support the benefits of using gravity inversion methods to model crustal structures. The different density contrasts in regions where volcanic processes have occurred provide optimal conditions to apply these gravity methods. In the case of the volcanic island of Gran Canaria, we used a new data set with a denser spatial distribution, which improves on the previous gravity studies. The new land gravity data set covers the whole island including previously unobserved areas. The marine data provided by U.S Geological Survey (Folger et al., 1990), helps to identify longer wavelength components of the gravity field and to define the structures near the coast. Applying our gravity inversion approach based on a genetic algorithm (Montesinos et al., 2005), we obtained a 3D model of the shallow sources of the gravity field, which are associated with prefixed density contrasts, reaching a depth of up to ∼20 km.

2. Volcanological and Geological Framework of Gran Canaria

The subcircular-shaped island of Gran Canaria with a diameter about 45 km is one of the largest islands of the Canary Archipelago. Its highest point with an elevation of 1,950 m (a.s.l.) is Pico de las Nieves, which is located near the center of the island (Figures 1 and 2). Using radioisotopic data from the oldest volcanic rocks outcropping in the different islands, McDougall and Schmincke (1976) suggested that the age of the archipelago decreases from east to west. The maximum age corresponding to Gran Canaria Island is ∼15 Ma. Geomorphologically, the island seems to be divided in two parts by a Pliocene rift zone that crosses it with northwest-southeast direction (Figure 2), which was first suggested by Bourcart and Jeremine (1937) (Rodriguez-Gonzalez et al., 2018; Troll & Carracedo, 2016). The southwest part of Gran Canaria, constituted by Miocene volcanic rocks, is called Paleocanaria and represents the oldest area. The northeast section of the island is called Neocanaria, and corresponds to recent volcanic rocks formed during the rejuvenation and youngest volcanic activity periods, dated as Plio-Quaternary. In the central part of the island, a Miocene caldera structure (Tejeda Caldera) associated with a well-developed central cone sheet swarm is found (e.g., Guillou et al., 2004; Rodriguez-Gonzalez et al., 2018; Troll & Carracedo, 2016).

The volcanic evolution of the island can be reviewed through several studies (e.g., Balcells et al., 1992; Carracedo et al., 2002; Guillou et al., 2004; Karátson et al., 2016; Menéndez et al., 2008; Rodriguez-Gonzalez et al., 2012, 2018; Schmincke, 1993). The present island's morphology is the result of several overlying

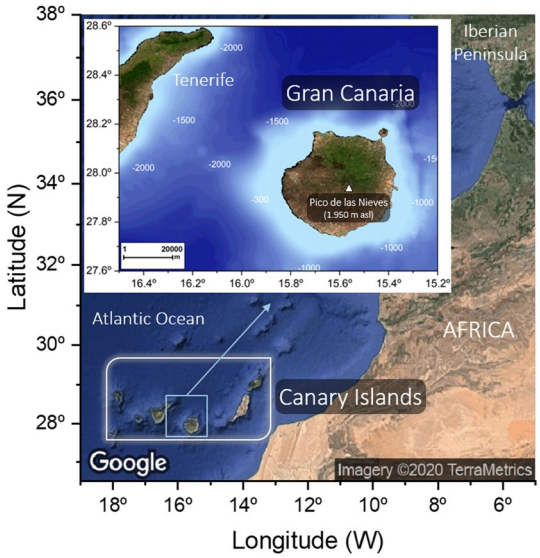

Figure 1. Location of Gran Canaria Island in the Canarian Archipelago (Spain). The inset shows an image of the island (orthophoto from OrtoPNOA 2018 CC-BY 4.0 scne. es) where the highest point is indicated with a white triangle (Pico de las Nieves at 1950 m a.s.l.). The bathymetry was taken from the GEBCO08 model (labels in meters). General view of the area obtained from Google Imagery TerraMetrics.

volcanic edifices corresponding to four major eruptive phases separated by two erosional intervals (Karátson et al., 2016) (Figure 2):

1. The oldest subaerial magmatic phase (between 14.5 and 13.5 My ago) was a basaltic shield building stage resulting in the development of a large shield volcano. This old edifice occupies the main area of the present island. The volume estimated for this shield volcano is of about 1,000 km^3 (Güigüí and Horgazales basalts) including related gravitational landslides. There are several hypotheses about the formation of the Gran Canaria shield. Balcells et al. (1992) and Troll et al. (2002) established the construction of the shield from just one eruptive center that would be located in the central part. However, Schmincke (1993) proposed the existence of three different eruptive centers: the first one would be located near the town of Agaete, in the northwest of Gran Canaria; the second one would be close to La Aldea village, in the west; and the third one would be located in the southeast, near the village of Agüimes (Figure 2). Schmincke and Sumita (1998) postulated a fourth emission center at the northeast of the island, close to the village of Arucas (Figure 2). This first stage continued with the eruption of the 14.0–13.3 Ma trachytic–rhyolitic Mogán ignimbrites, with vertical caldera collapse and felsic post-caldera volcanic activity resulting in the formation of a large cone sheet (Tejeda caldera), which is located in the western-central part of the island. Explosive and violent eruptions followed as the shallow reservoir gradually developed to a rhyolitic composition with a recurrent magma supply from the subjacent basaltic chamber.
2. The second phase started with the eruption of the Montaña Horno rocks, dated between 13.3 and 13.0 Ma and with a trachyphonolitic composition. After this, pyroclastic rocks and lava flows of the same composition as Montaña Horno were deposited. They constitute the Fataga Group that has been dated between 12.4 and 8.8 Ma, and that could be part of a central stratovolcano. From 8.8 to 5.5 Ma, a rest period resulted in the erosion of the volcanic reliefs and the sedimentation of an important sedimentary detrital Formation (Las Palmas Fm) (Guillou et al., 2004; Pérez-Torrado et al., 1995).
3. A new period of volcanic activity developed from 4.9 to 2.6 Ma. During this period, a large stratovolcano (Roque Nublo) composed of pyroclastic rocks and lavas of basanitic and trachitic to phonolitic composition grew into the central part of the island. The Roque Nublo edifice experienced several major collapses that were followed by a new period of activity (Post Roque Nublo volcanism) (Pérez-Torrado et al., 1995). This stage finished with a new erosional period whose duration is less than 1 Ma.
4. The last stage of volcanic activity corresponds to the Post-Roque Nublo volcanism developed from 3.0 Ma to 3 ka (Holocene). This volcanic activity resulted in the formation of a monogenetic volcanic field comprising up to 24 small cones restricted to the northeast of the island (Rodriguez-Gonzalez et al., 2018). It has been proposed (e.g., Guillou et al., 2004) that this volcanism was related to a rift zone trending NW-SE with an eastward migration of the activity during the Holocene. There are no reports of submarine eruptions related to this period. Previous works (e.g., Balcells et al., 1990) have pointed out the existence of lineaments trending 110°N–120°E that are outlined by the alignments of the volcanic cones corresponding to this stage (Figure 2). The authors proposed that deep fissures, only detectable by the cone alignments, must exist, acting as feeder zones.

A distinctive feature of the Holocene volcanic activity is that the lava flows run along ravine beds. This Quaternary volcanism continued intermittently occurring exclusively in the northeastern part of Gran Canaria (e.g., Carracedo et al., 2002; Rodriguez-Gonzalez et al., 2009). The Quaternary volcanic activity is probably in a preliminary stage (Hoernle & Schmincke, 1993), whereas the older Miocene edifice corresponds to a subaerial magmatic phase. Thus, the only volcanic stage that is fully exposed corresponds to the Pliocene volcanism. Regarding the evolution of the island, Carracedo (1999) suggested that Gran Canaria is presently in the post-erosional stage.

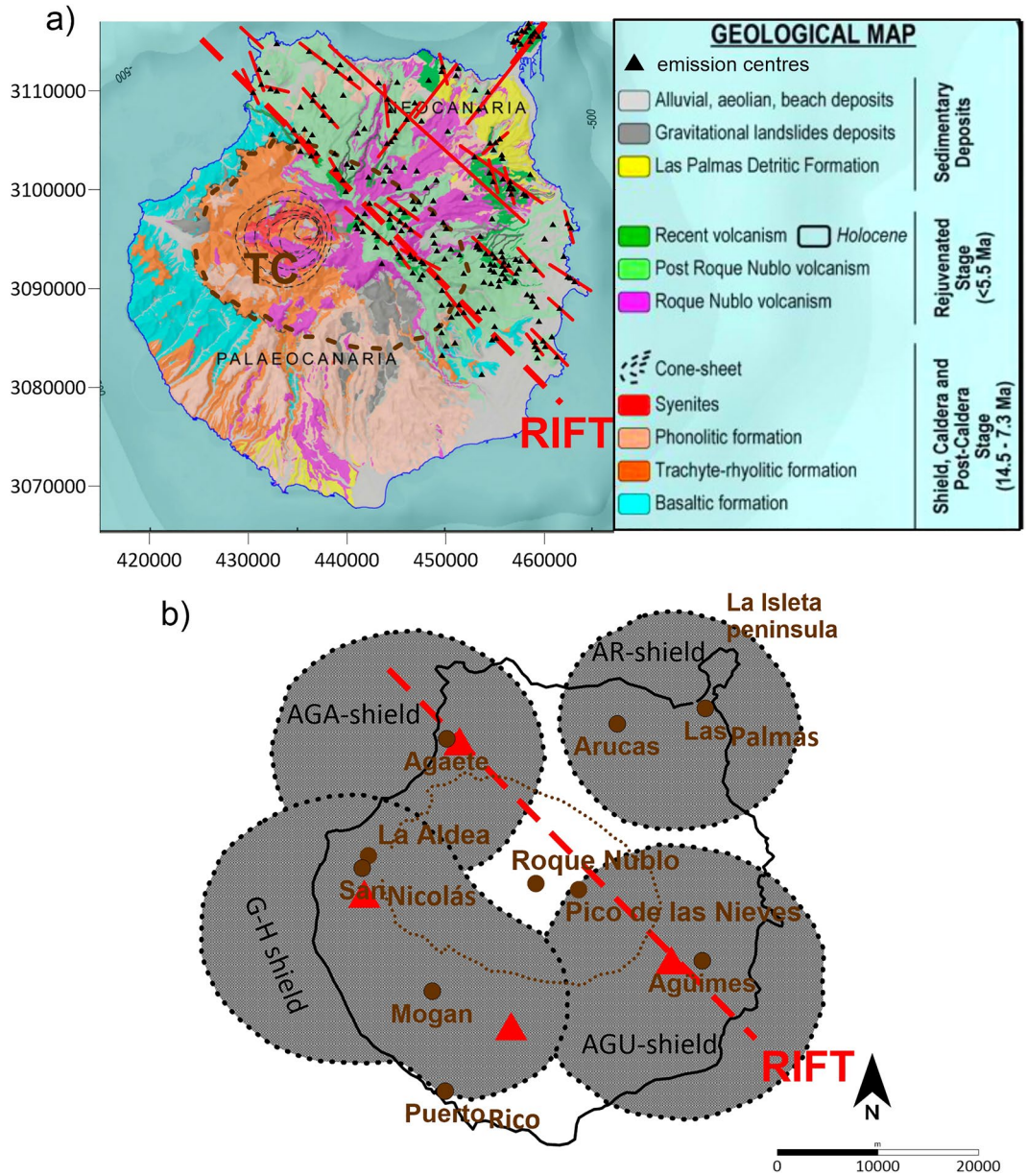

Figure 2. (a) Simplified geological map of Gran Canaria displaying the distribution of major volcano-stratigraphic units and related structures (modified from Rodriguez-Gonzalez et al., 2018 and Barrera & García Moral, 2011). The main geomorphological features are divided into two parts (Palaeocanaria and Neocanaria) by the Pliocene rift zone (red dotted line). The red lines represent structural lineaments inferred from geological data and the location of volcanic emission centers (black triangles) from Post-Roque Nublo and recent volcanism stages in Neocanaria (Balcells et al., 1990). The Miocene Tejeda Caldera (TC) (brown dots circled area) and the central cone-sheet swarm (black dotted lines) are shown. UTM coordinates are given in meters (Zone 28N). (b) Speculative locations of Güigüi-Horgazales (G-H), Agüimes (AGU), Agaete (AGA) and (highly conjectured) Arucas (AR) shields by Schmincke and Sumita (1998). There is a coincidence between these possible Miocene shield volcanoes and high gravity anomalies (red triangles) (Figure 3), except for the case of the Arucas shield. Some locations are indicated with brown dots (see text).

The lithospheric structure of Gran Canaria is similar to other islands of the Archipelago. The top layer is composed of alternating lava flows and pyroclastic deposits. The second layer corresponds to oceanic sediments preceding the volcanic activity. Finally, the third and four layers correspond to the basaltic oceanic crust and the lithosphere mantle, respectively. This lithospheric structure was studied by Ye et al. (1999) and Krastel and Schmincke (2002), estimating a Moho depth of 15 km at the northern part of the island by means of reflection

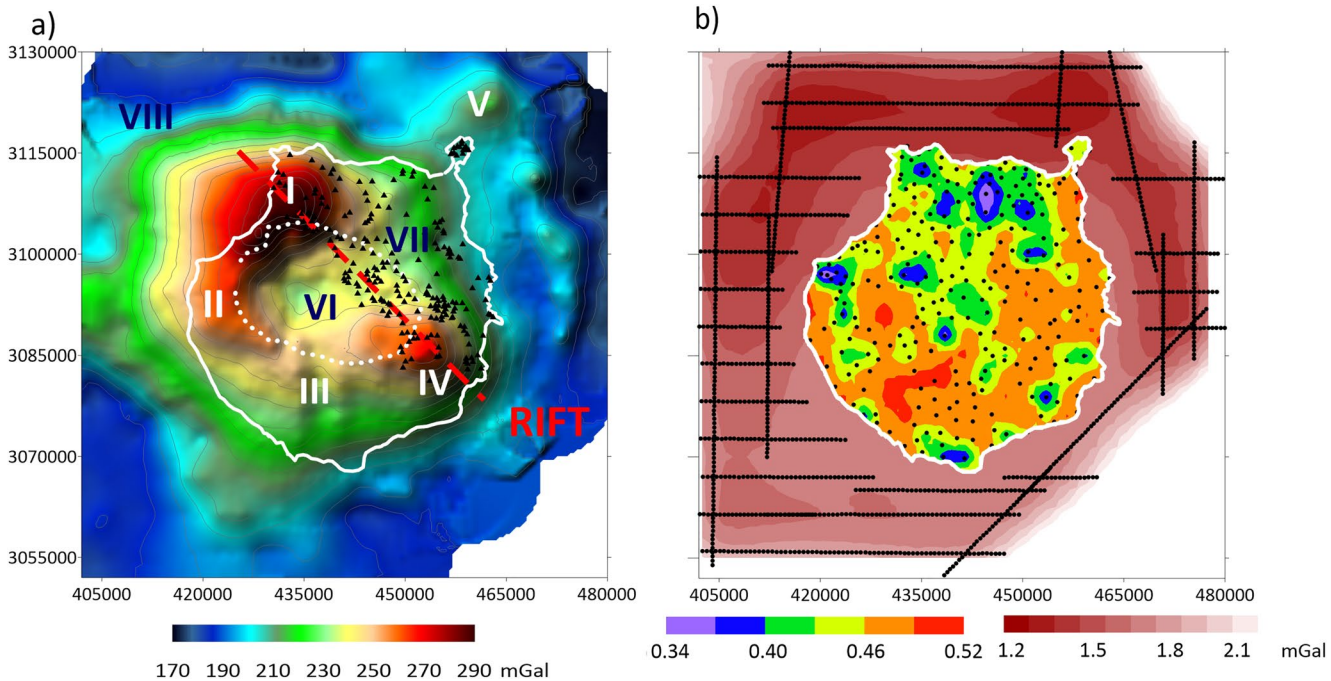

Figure 3. (a) Map of Bouguer anomaly of Gran Canaria. The main gravity high values are identified by white numbers (I to V) and the gravity lows by black numbers (VI to VIII). Other features are indicated: margin of Tejeda Caldera (white dots circled area), emission centers in the Neocanaria area (black triangles), rift zone (red dotted line). (b) Uncertainty estimate for land and marine gravity datasets (different color scales). The black points show the location of gravity stations. The UTM coordinates are displayed in meters (Zone 28N).

and refraction seismic data. Martínez-Arévalo et al. (2013) found a crustal thickness of 23.5 km for Gran Canaria Island, although they erroneously established concordance with the results of Krastel and Schmincke (2002) and Blanco-Montenegro et al. (2003). Blanco-Montenegro et al. (2003) argue that rocks located at a depth ranging from the Moho to ~23 km would act as magnetic and estimated a Moho depth of 15 km. According to Krastel and Schmincke (2002), the crustal structure of Gran Canaria is heterogeneous and exhibits major lateral variation of *P*-wave velocities, with values higher than 5.5 km/s in general. The highest velocity values are located near the proposed eruptive centers of the Miocene shield volcano previously described, as well as at the location of the Pliocene Roque Nublo volcano. The authors suggest that this heterogeneous structure with high *P*-wave velocities is the result of large amounts of high-density intrusives.

3. Bouguer Gravity Anomaly Map

In this paper, we improve the previous gravity maps of Gran Canaria (Bosshard & MacFarlane, 1970; Camacho et al., 2000), which do not cover the entire island, using a new land gravity data set and previously available marine gravity data surrounding the island. We observed 263 new land gravity stations (Figure 3) using a Scintrex-CG5 gravimeter recording at 1 min intervals for about 30 min at each station. Then, 21% of these stations were re-observed to ensure drift corrections and a good fit among the five surveys performed between the years 2012–2014. The positions of the stations, which are conditioned by the topography, were calculated using GPS observations with post-processing differential correction. The average distance of contiguous gravity stations is nearly 2–3 km (Figure 3). A tidal model obtained from gravity tide observations achieved in various islands of the Archipelago (Arnoso et al., 2011) was used to correct the land gravity data. After the usual corrections of instrumental drift, jumps and tides, the adjustment of the observations shows a standard deviation of 0.012 mGal (1 mGal = 10^{-5} m s^{-2}). All the gravity values are referred to IGSN 1971.

Gravity studies on islands might be improved by including marine gravity values to define the prolongation or border of the anomalies near the coast. In this case, we used 363 marine gravity values from the U.S Geological Survey (Folger et al., 1990) up to 10–40 km from the coastline, according to availability (Figure 3).

The terrain effect on the gravity data was corrected up to 150 km away from each station considering a digital terrain model at a scale of 1:25,000 (National Geographic Institute of Spain) and bathymetric data from ETOPO1 of the National Geophysical Data Center (Amante & Eakins, 2009). The terrain density value was determined from a range of values according to previous information, as it is explained below and by looking for a better final adjustment of the observed anomaly by the inversion process. We selected 2,600 kg/m^3 as an adequate value to represent the average of the terrain and Bouguer cap density for the island, and a density of 1,027 kg/m^3 in the case of seawater. Taking into account the similarity of the volcanism among the islands of this archipelago, this terrain density is closer to the density values used in other gravity studies in the Canaries: 2,500 kg/m^3 for Fuerteventura, 2,510 kg/m^3 for El Hierro, 2,500 kg/m^3 for Tenerife (Montesinos et al., 2005, 2006; Sainz-Maza Aparicio et al., 2019), etc. This density value is also in agreement with the infill density used by Collier and Watts (2001) and Watts (2000) in their crustal study with seismic refraction data. Finally, the crustal structure study of Krastel and Schmincke (2002) provides a mean value of around 5 km/s in the shallowest layer of the *P*-wave velocity model in this island. This velocity could be related to a density value of 2,570 kg/m^3 (Barton, 1986). Therefore, the value of 2,600 kg/m^3 for the terrain correction appears adequate to calculate the new complete Bouguer gravity anomaly map for Gran Canaria (Figure 3).

The quality of the land and marine gravity data set was evaluated by a covariance analysis from all observations data. This method makes it possible to separate correlated signal levels and noise (e.g., Montesinos et al., 2005). Thus, the standard deviation of the estimated non-correlated noise (0.271 mGal) can be considered an evaluation of the quality of the final map. The uncertainties in the observations and in some corrections (the use of a single density value in the terrain correction, etc.) and/or the very short wavelength anomalies that do not achieve the correlation level identified by this analysis, could be the cause of this noise.

This process was also used to evaluate the relative quality in function of the stations distribution from the uncertainty in the estimation of the correlated signal of this map. We have obtained different levels of uncertainty for the land and marine data because they can be considered as sets with diverse resolution, characteristics and accuracy. We have estimated the uncertainty in the signal of the longest wavelength including the marine data (it corresponds to the deepest sources) and the error in the signal of the medium wavelengths of land data (it corresponds to sources at shallower depths). Both uncertainty distributions are overlapped in the same figure (Figure 3b), and they are useful to weigh the observations in the inversion process. This relative uncertainty map appears conditioned mainly by the distribution of stations, and they cannot be considered as absolute uncertainties. To plot this map, we defined a grid of 157 × 157 nodes with a spacing of 500 m. The interpolation was calculated using the Kriging method with automatic variogram fitting and a search neighborhood restricted to eight points. All the maps shown in this paper were plotted using Surfer (Golden Software LLC.).

Therefore, this new gravity anomaly map improves considerably from the previous ones because it covers large regions where no data were available to date. This means, as it can be seen from the uncertainty distribution maps, that the higher spatial density of the survey increased its accuracy and, furthermore, allows the study of structures related to volcanic processes that had not been previously considered.

The Bouguer gravity anomaly map ranges by 120 mGal and has maximum values at the NW, W, and SE sectors of the island surrounding a gravity low in the central area (I, II, III, IV and V respectively in Figure 3). The offshore prolongation of the maximum anomalies at the NW and W areas (I and II in Figure 3) is well defined by the marine gravity data. The maximum values of anomalies I and IV (Figure 3) are just located at the rift that crosses the island. Anomaly III is a weak gravity high located in a gradient zone. The three main gravity highs are extended toward the areas where the formation of the basaltic shield volcano took place, throughout the border of the Tejeda caldera, which exhibits the lowest gravity anomaly values (VI in Figure 3). The NE area (Neocanaria), which concentrates the Plio-Quaternary volcanism, is characterized by a gravity gradient trending SW-NE, perhaps slightly disturbed by different phases in the rejuvenated volcanism stage, and it is associated with a low gravity zone (VII in Figure 3).

In the offshore zone, this study reveals a gravity high (V in Figure 3) located near the small peninsula called La Isleta, and a low anomaly zone in the NW area of the map (VIII in Figure 3). Both features of the gravity map show a clear correlation with the reduced pole magnetic map calculated from aeromagnetic data by Blanco-Montenegro et al. (2003, 2018).

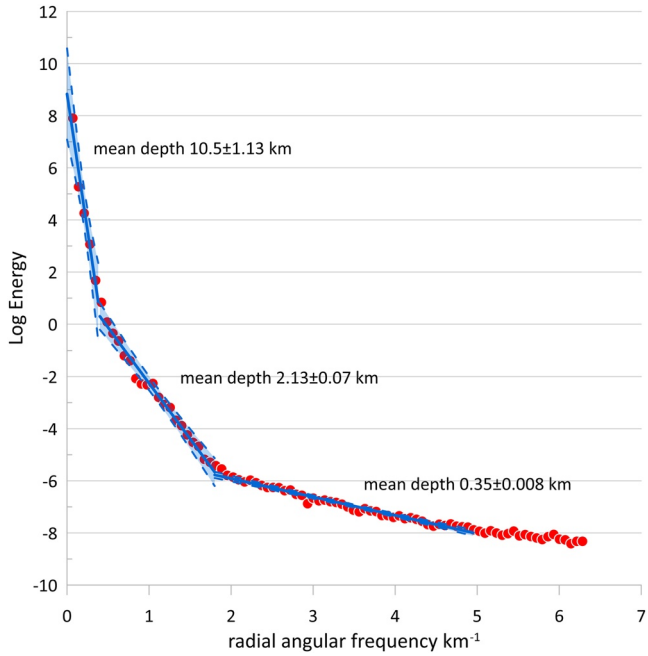

Figure 4. Plot of the logarithm of the power spectrum of the Bouguer anomaly versus radial angular frequency. Three different linear segments, corresponding to causative sources located at mean depths of ∼10.5, ∼2.1, and ∼0.35 km are obtained. The blue areas represent the 95% confidence interval for the computation of the linear fit.

There is no clear linear regional trend in this map suggesting, for instance, the existence of a linear variation in the thickness/density of the subsurface layers at a regional scale. In addition, any possible non-linear trend sampled by our data could reflect the effects of the deepest structures, which are particularly interesting for our study. Therefore, we use our gravity inversion method to identify these sources of the gravity field, without removing any regional component.

We have also performed a spectral analysis to obtain more information about the mean depths of the different sources contributing to the gravity anomaly. This is a classical statistical approach proposed by Spector and Grant (1970) based on the computation of the natural logarithm of the energy of the anomaly from Fourier Transform. When this value is plotted versus the angular frequency, a decay in energy with frequency is observed and can be approximated to a straight line whose slope is related to the mean depth of the source (Syberg, 1972). Figure 4 shows the result of the analysis, where three different linear segments can be observed. The first segment corresponds to a source located at 10.5 ± 1.13 km depth and would be considered as the regional source of the area. This mean depth agrees well with the Moho depth at oceanic areas (∼11–12 km depth, e.g., Banda et al., 1981), but is shallower than the 15 km depth obtained for Gran Canaria from seismic and magnetic studies (Blanco-Montenegro et al., 2003; Krastel & Schmincke, 2002; Ye et al., 1999) The discrepancy could be explained by the fact that the spectral depth estimation is a mean value biased toward the typical depth of the Moho in oceanic areas and/or to the small window size of the anomaly map that could not contain all the long wavelengths related to the Moho geometry. Related to this, another possibility is that ∼10–11 km depth detected would be really associated not to the Moho, but to the upper-lower crust boundary detected by Ye at al. (1999) and Krastel and Schmincke (2002), both of them defining this major crustal boundary at ∼10 km depth. The second segment corresponds to a source located at a mean depth of 2.13 ± 0.07 km depth and a third linear segment associated to a 0.35 ± 0.008 km depth would be related to the effect of the shallowest bodies (e.g., monogenetic volcanoes). This analysis, identifying different depth levels of the gravity sources, will be supported by the results of the following inversion process.

4. Gravity Inversion Model

Our inversion approach follows the procedure of the genetic algorithms that search the optimum solution using a strategy that takes inspiration from the principle of evolution by natural selection. These algorithms modify in an evolutive process a set of possible solutions (models), which are considered as a population of individuals. This population evolves by changing the parameters that define each individual, seeking to minimize an error function, which determines the quality of the solution. After an iterative process where new generations of individuals are created and evaluated, the individual that minimizes this error function is considered as the best solution to the stated problem (e.g., García-Martínez et al., 2018; Montesinos et al., 2005). The non-uniqueness of the solution of the inversion problem in potential fields is the main difficulty that appears when we reproduce the observed gravity data identifying the sources of this field. This problem has to be solved, for instance, using geological, geophysical and mathematical constraints that help us to choose the best solution among different possibilities. Thus, to avoid the problem of non-uniqueness in the inversion process to determine the geometry of the sources of gravity field, we use an adequate error function and q values of positive and negative density contrasts, which correspond to these sources, fixed as constraints. The error function, F, is defined by the misfit between the observed and modeled gravity field, and it also depends on the mass of the sources of the model (Montesinos et al., 2005),

$$\boldsymbol{F}(\boldsymbol{m}_k) = \left(\boldsymbol{A}\boldsymbol{m}_k - \boldsymbol{g}_{\text{obs}} - G_k\boldsymbol{u}\right)^T \boldsymbol{E}_{\text{ss}}^{-1} \left(\boldsymbol{A}\boldsymbol{m}_k - \boldsymbol{g}_{\text{obs}} - G_k\boldsymbol{u}\right) + \beta \boldsymbol{m}_k^T \boldsymbol{C}_m \boldsymbol{m}_k \quad (1)$$

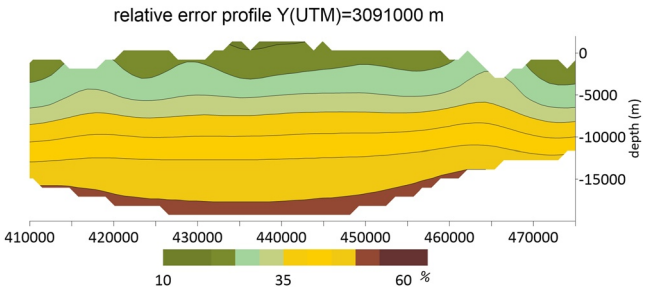

Figure 5. Relative error (in %) associated with the model according to the position of the prisms, and its contribution to the calculated gravity field (inversely proportional), represented along the profile $Y = 3091000$ (UTM coordinate, Zone 28N).

where $\boldsymbol{g}_{\mathbf{obs}}$ corresponds to the gravity data in their observation sites, $\boldsymbol{A}$ defines the direct problem, $\boldsymbol{E}_{\mathbf{ss}}$ is the matrix of the data error, G_k is a constant term obtained from the weighted media residual, $\boldsymbol{u}$ is the unitary vector, β is a regularization parameter chosen a priori, and the $m \times m$ matrix $\boldsymbol{C}_{\boldsymbol{M}}$ describes the uncertainty of the model m_k.

To define each model, we divide the subsurface volume of the studied area into a three-dimensional grid of M regular prisms. Then, by means of an iterative process based on a genetic algorithm, the possible models of the sources of the gravity field are defined allocating to each cell one of the q a priori fixed density contrasts. From an initial set of possible models of solutions (population), the algorithm acts iteratively by altering these models by mutation, cross and smoothness operators. The genetic algorithm is a global optimization procedure that provides a final solution that is independent of this initial population of models (e.g., Michalewicz, 1994). Thus, we use an initial population where all prisms have null density contrast. These initial models evolve throughout the iterative process, where the best models are survivors. The main usefulness of the smoothing technique is to avoid very small, isolated structures and the excess of the total anomalous mass. Each model of the population is evaluated by the error function, which determines if the genetic operators act and whether this model is a survivor in the evolution process, or if it is removed. At the end of this process, the best survivor corresponds to the model of the population that minimizes the error function. More details about this process can be found in several published applications (e.g., Montesinos et al., 2005; Sainz-Maza Aparicio et al., 2019, etc.).

In this case, the model is parameterized as a set of 47,016 regular prisms with sides of 1,500 m, distributed from 1,000 m below the topographic surface to the bottom of the model at 25,000 m depth. As it is usual in the gravity inversion (e.g., Long & Kaufmann, 2013), the parameterization of the model was chosen based on the average distance between contiguous stations and on the size of the survey area across the island.

We have fixed the possible density contrasts ranging between −300 and +400 kg/m^3 to estimate the geometry of the sources of the gravity field. This empirical selection was based on the typical density values of volcanic rocks of the Canary Islands (e.g., González de Vallejo et al., 2008; Rodríguez-Losada et al., 2009) and supported by other successful gravity studies in this area (e.g., Camacho et al., 2000; Montesinos et al., 2006, 2011; Sainz-Maza Aparicio et al., 2019). These values are in agreement with density estimates for successive layers representing the crust in Gran Canaria: 2.6 g/cm^3 for sedimentary rocks (depths from 0 to 2 km), 2.8 g/cm^3 for the intrusive volcanic edifice (depths from 2 to 10 km), 2.9 g/cm^3 for the intrusive oceanic crust (depths from 10 to 15 km), and 3.4 g/cm^3 for the mantle (from 15 km down) (Jensen, 2016). A proof of the suitability of the range of selected density contrasts for the inversion is the good definition of the sources geometry in the model, consisting of compact and well-developed volumes rather than many small, isolated bodies.

Because the marine and land gravity data have different accuracies and resolutions, the residuals of the fit are weighted by the relative error estimated from covariance analysis (Figure 3). In addition, the uncertainty of the gravimetric prospecting method versus the depth of the model is considered in the error function by including a second term. This term corresponds to an evaluation of the source masses weighted by the position of each prism, which defines the percentage of relative error in the model (Figure 5) (e.g., Camacho et al., 2000; Montesinos et al., 2005).

5. Results

The application of the gravity inversion provides the best solution model with a composition of the fixed density contrasts, which represent the gravity field sources that fit the observed data resulting in a Gaussian error distribution with a standard deviation of 1.12 mGal (Figure 6). The final residual of the inversion process (difference between the observed and the modeled gravity field) contains the effect of the uncertainty of the measurements, those effects that were not completely corrected (e.g., topographic masses) as well as very local anomalies for which inversion was not attainable due to the resolution of the model.

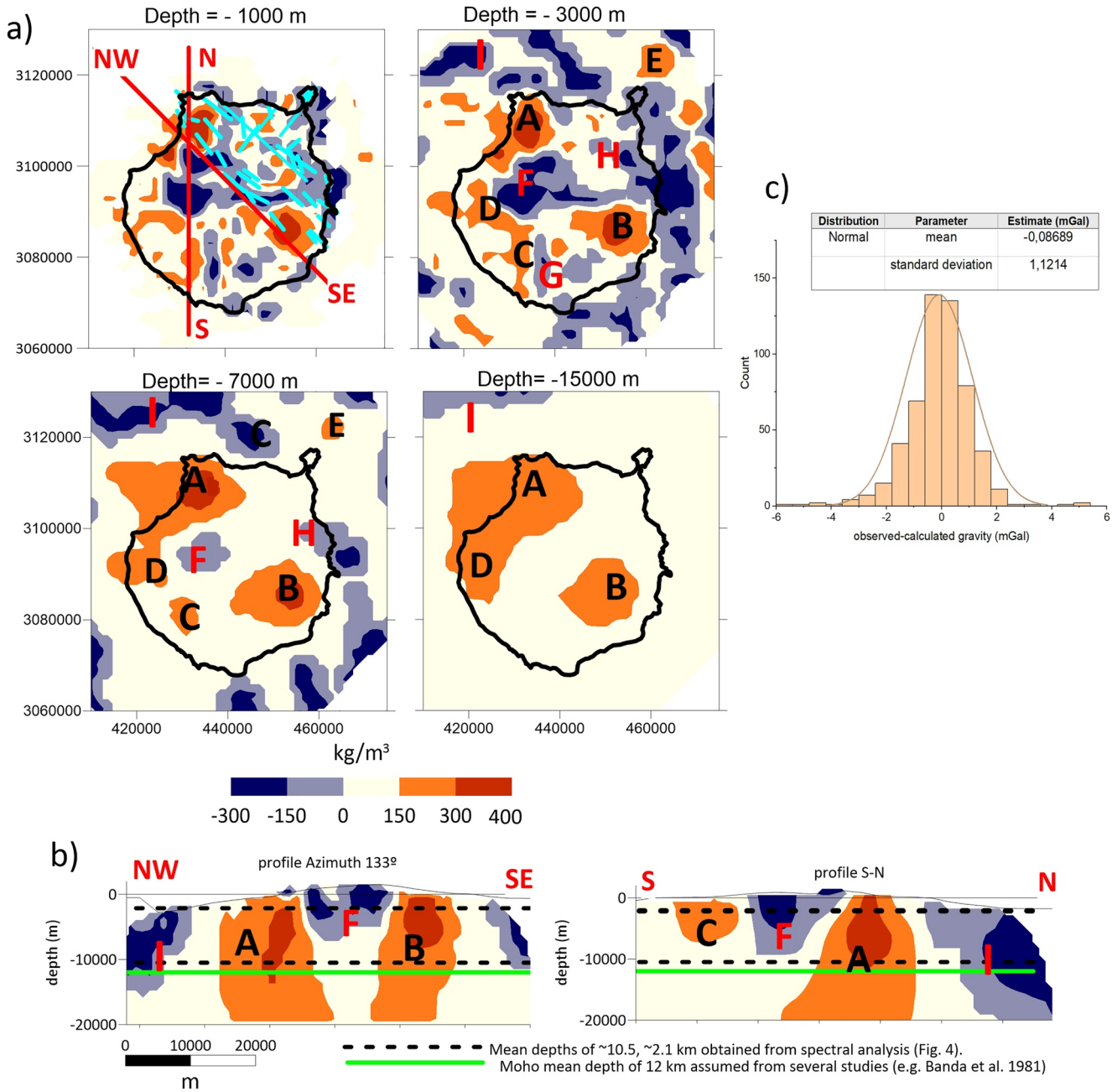

Figure 6. Model of the density contrasts calculated from the gravity inversion. The values range between −300 and 400 kg/m^3. The capital letters indicate the locations of different structures referenced in the text. Cyan lines indicate several lineaments inferred from the emission centers (Balcells et al., 1990). The UTM coordinates are given in meters (Zone 28N). (a) Several horizontal sections of the model from 1,000 to 15,000 m depth are shown. (b) Two vertical sections of the model following the rift direction (left) and the N-S direction crossing the Caldera Tejeda (right). (c) Histogram of the residual obtained from the inversion process (observed gravity minus calculated gravity).

Figure 6 displays this model through several horizontal and vertical sections, where the main gravity sources have been identified by letters. The genetic algorithm has allowed us to obtain a detailed model of subsurface density structures for the depths 1,000–20,000 m below the surface. Then, the inversion process identifies the gravity sources at a higher level than the initial parameterization at 25,000 m, this being the maximum depth of the modeling allowed by the extension of the survey and the features of the long-wavelength gravity signal. These structures are related to the volcanic evolution and the geological framework of the island (Figures 6 and 7). High

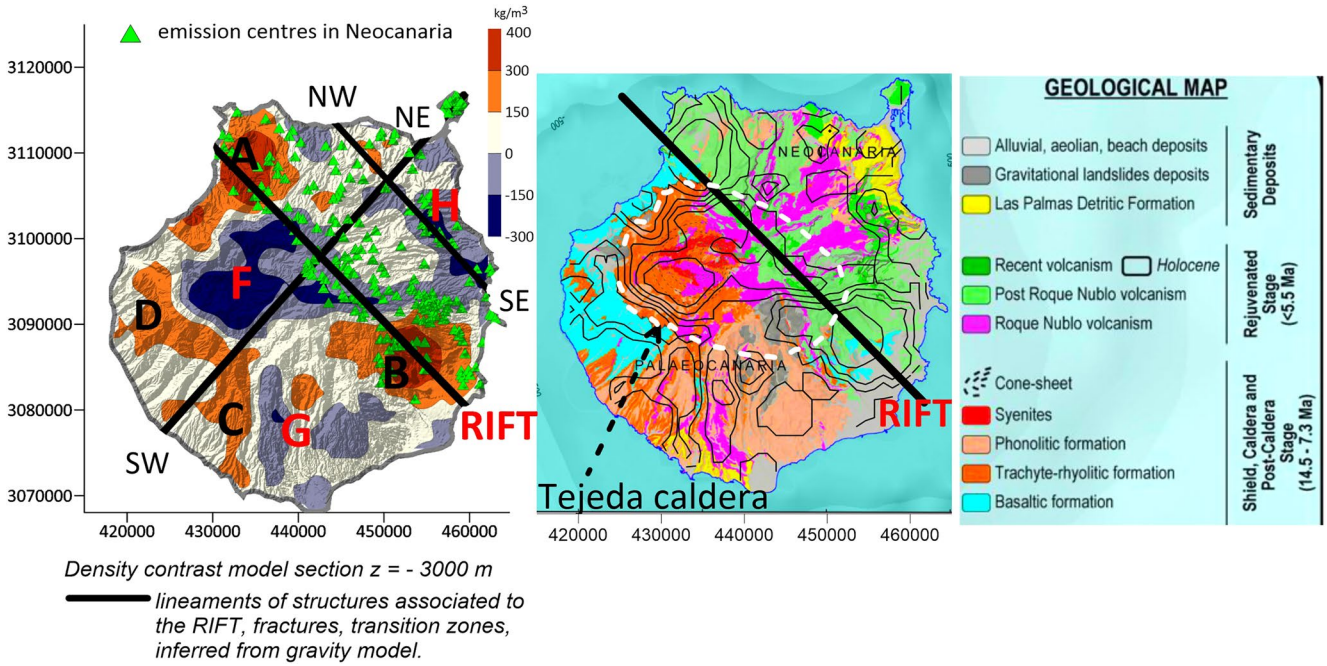

Figure 7. Density contrast model section at 3,000 m depth overlying the digital elevation model (left) and contour lines of the density contrast model overlying the geological map (right). The left pane shows the emission centers (green triangles) and several possible lineaments (black lines) associated to the RIFT and transition zones in the density contrast distribution model. The UTM coordinates are given in meters (Zone 28N).

densities are mainly found beneath the basaltic and phonolitic formations. The structure beneath Tejeda caldera and the area of the alignments of Plioquaternary volcanoes have primarily low density.

Two deep bodies with positive density contrast dominate the model and define the main structure of the island. These dense bodies (A and B in Figure 6), located in the NW and in the SE of Gran Canaria, appear in the shallow sections but they extend in depth toward the base of the crust. They correlate well with outcrops of the basaltic shield stage of the island, which was the most important stage in the construction of the subaerial edifice and responsible for more than 90% of its volume.

A third dense source (C in Figure 6) is revealed to the south in correspondence with a small and narrow outcrop of the old shield basalts (Figures 2 and 7).

The dense structure identified by D in the model (Figure 6) is clearly associated with the Miocene volcanism, and it appears as an extension of body A toward the SW from the deepest section of the model.

The gravity model also evidences a low-density, round structure in the center of Gran Canaria (F in Figure 6), extending from 7,000 m depth to the surface, between the two dense bodies A and B. This structure is restricted to shallower depths, and its location corresponds to the Tejeda caldera and the outcrops of trachy-phonolitic and syenitic materials in the central part of Gran Canaria that were emplaced after the shield basaltic stage. A secondary shallow low-density structure (G in Figure 6), revealed to the South of body F, could be also related to this building stage of the central volcanic edifice.

Figure 6 shows several linear trends of low-density sources at depths shallower than 3,000 m. Their main orientations are E-W and NW-SE, the latter being easily recognized at the NE part of the island (see H in Figure 6). They can be related to the outcrop of the more recent Holocene volcanism that is widespread in this area.

Regarding the offshore areas, two main sources can be outlined. To the NE of the La Isleta peninsula, the gravity inversion reveals a circular, dense structure (E in Figure 6) at depths between 3,000 and 7,000 m b.s.l. In addition, a low-density, elongated structure is identified to the NW of the island (I in Figure 6) from 3,000 m of depth to deepest sections of the model. A geological interpretation for these structures will be proposed in the Discussion section.

Respect to the mean depth of the sources identified by spectral analysis (Figure 4), the deep and intermediate levels (at mean depths of 10.5 and 2.13 km, respectively) correspond with the depth range within which the most significant gravity sources were identified by our modeling (Figure 6). The intermediate level (2.13 km depth) could be related to the gravity effect of the sediment layer and/or the top of the high and low-density bodies obtained in the gravity inversion models (Figure 6b). Finally, the shallowest level at 0.35 km depth could be related to the effect of the shallowest bodies (e.g., monogenetic volcanoes), which are not identified in the model.

6. Discussion

The crustal structures identified by the gravity inversion are modeled as a distribution of density contrasts with respect to their surroundings and they can be associated with the different stages which have characterized volcanism on the island. The two main high-density structures (A and B in Figure 6) located from 20,000 m depth to the surface in the density model could be interpreted as plutonic complexes emplaced during the early volcanic history of Gran Canaria and the feeding system of the Miocene volcanic edifices whose remains presently outcrop as basalts, with a higher density than the surrounding trachytic, phonolitic, syenitic and pyroclastic rocks. The geometry of these high-density structures could be related to the presence of intrusive bodies derived from mantle melting reaching the shallowest levels of the crust. After solidification, they would constitute mafic plutonic bodies with a density similar to the oldest basaltic Miocene rocks. The high-density source C, located in the southern part of the island, could be also related with the intrusive core emplaced in the early formation stage of the island, although recent felsic volcanic materials covered the early subaerial shield basalts in this area. These three structures (A, B, and C) were also revealed by aeromagnetic data and interpreted in the same way (Blanco-Montenegro et al., 2003). This correlation confirms that these intrusive bodies are both denser and more intensely magnetized than the surrounding materials. These dense structures are deeply rooted in the crust (see the horizontal section at 15,000 m b.s.l. in Figure 6a) where body D appears to be connected with body A, being the same plutonic structure in the deep crust.

Several authors have studied the mantle xenoliths found in different volcanic materials of the Canary Islands to obtain information about the conditions of pressure, temperature and depth at which the magma is formed. Aulinas et al. (2010) suggested that magma ascent occurred in several stages: a main deep level within the upper mantle (between 22 and 17 km), and a secondary intermediate level in the crust (from 8 to 1.5 km) where the crystallization of mafic magmas took place, whereas evolved magmas accumulated at crustal depths within the range from 15 to 3 km. The gravity inversion model does not identify the levels where the magma was stored. However, these levels coincide with the presence of high-density bodies that can be associated to the magma storage.

Previous geophysical studies also suggest the existence of the dense bodies identified by our gravity inversion. For instance, these high-density bodies are in agreement with the high resistivity structures crossing the island recently identified by magnetotelluric inversion (Ledo et al., 2021). Moreover, the geometry of these dense structures supports the hypothesis of Schmincke (1993), who proposed that the building of the shield basaltic edifice developed through three main eruptive centers, identifying several possible Miocene shield volcanoes (Figures 2 and 6): the Agaete shield (associated with gravity source A), the Güigüi-Horgazales shield (in correspondence with the gravity source D) and a third Agüimes shield (linked to the gravity source B). The deep roots of the plutonic bodies A and B indicate that the emission centers of Agaete and Agüimes were the most important ones during the early growth of Gran Canaria. In addition, our work points out the presence of a fourth minor emission center to the south, which is related to the Güigüi-Horgazales shield (associated with gravity source C). However, we do not find evidence of the eruptive center near Arucas in the NE of Gran Canaria as proposed by Schmincke and Sumita (1998), since no significant gravity anomaly was revealed in that area.

At the end of the shield basaltic stage, large volumes of trachytic-rhyolitic materials were erupted and followed by the collapse of the Tejeda Caldera and felsic post-caldera volcanic activity in the central part of the island. The low-density body F (Figure 6) may be associated with the syenitic core of this felsic volcanic edifice, also identified by the seismic data of Ye et al. (1999) and the aeromagnetic study of Blanco-Montenegro et al. (2003). In the next volcanic cycle (Pliocene), a great stratocone was emplaced, suffering subsequent erosion and collapse (~3.5 My ago). Its remains constitute the Roque de Nublo Group, which is presently seen around the Tejeda collapse caldera. The elongation of structure F in the shallowest sections and the low-density structure in the southern area (G in Figure 6), which have a signature only in these sections of the model, would be associated with this rejuvenated stage of Roque Nublo volcanism (Figure 7).

Other low-density structures found up to 4,000 m in depth in the gravity model (for instance H in Figure 6) define some structural trends that match the orientation of the fractures acting as feeder dikes of the different monogenetic volcanoes originated during the Post-Roque Nublo volcanic activity phase developed in the northeastern half of the island (see Figure 7 and Section 2 of this work), whose existence has been proposed by other authors (Balcells et al., 1990; Guillou et al., 2004; Rodriguez-Gonzalez et al., 2018). In these shallowest sections of the model, it can be observed that the Rift zone crosses some low-density areas that could be associated with fractured rocks and probably to the presence of clays and fluids related to hydrothermal alteration (Figures 6 and 7).

In the NE offshore, the high-density body E could be related with a Quaternary submarine volcano identified by Funck and Schmincke (1998) using high-resolution bathymetry data. Krastel and Schmincke (2002) interpreted this zone, from active seismic tomography, as a volcanic rift zone with a great quantity of dikes. This correlation suggests that this dense, vertical source of the gravity field represents the feeding system of this submarine volcano.

The low-density elongated structure identified offshore to the NW of the island (I in Figure 6) from 3,000 m of depth to deepest sections of the model may have a tectonic origin, as will be explained below in more detail.

From a tectonic perspective, the gravity inversion shows a clear correlation between the Rift, which separates the two different domains defined on the island (Neocanaria and Palaeocanaria) and zones of transition in the density distribution model, which could be weakness zones used by the magma to reach the surface. This Rift connects the two main remnants of the Old shield Miocene edifice (bodies A and B in Figures 6 and 7), suggesting that this fracture acted as the feeder zone of the old basaltic Miocene shield volcano and, consequently, has been active since the last 15 My. Furthermore, both old stratovolcanoes corresponding to the volcanic phases 2 and 3 are also located near this rift zone. Also, the most recent volcanism in the island started in the vicinity of this lineament. Therefore, it can be concluded that the Rift is the most important volcano-tectonic structure of Gran Canaria Island and represents a long-lived extensional fracture zone that has controlled the volcanic activity at least since the Miocene.

Although this NW-SE fracture is clearly the more important tectonic feature of the subaerial edifice of Gran Canaria, this is not the only one. Several works (e.g., Balcells et al., 1990, 1992; Hansen, 2009; Mangas et al., 2002; Rodriguez-Gonzalez, A., 2009) have pointed out the presence of several fractures trending NW-SE parallel to the major rift structure and extending toward the eastern coast, as well as a second system trending NE-SW to ENE-WSW, clearly visible at least at the La Isleta Peninsula (Figure 2). These fractures do not outcrop because they are covered by more recent volcanic and sedimentary rocks, but they can be inferred from the alignment of volcanic emission centers. By combining geological, radiometric dating and geomorphological information, a spatio-temporal migration of the volcanic activity from the rift structure toward the NE following the different NW-SE fractures has been proposed (Balcells et al., 1990, 1992; Mangas et al., 2002). The NW-SE system can be recognized as shallow low-density structures (see H in Figures 6 and 7). The NE-SW lineament may be inferred in the model if the main transition zones between different low and high-density bodies are considered (Figure 7). This lineament runs along of the boundaries of low-density bodies located in the north zone, along the boundary of low-density body F, and also where the C and D high-density bodies appear joined with different orientation (Figure 7). Although the structures identified close to the edges of the model should be interpreted with caution, the elongated low-density structure trending ENE-WSW (I in Figure 6), situated over the NW submarine edifice coincides with the major crustal fracture associated with the submarine growth of the island revealed in the magnetic study achieved by Blanco-Montenegro et al. (2018) and suggested for the first time by Bosshard and MacFarlane (1970). Thus, all these results provide evidence that tectonic activity has performed an important role in the volcanic history of Gran Canaria, in agreement with the models proposed to explain the volcanic origin of the Canary Islands where tectonics play the main role (Section 1).

7. Conclusions

A model of the crustal structures of Gran Canaria Island has been revealed by the inversion of a new gravity data set. The new Bouguer gravity anomaly map calculated for Gran Canaria (Figure 3) considerably improves the previous ones (Bosshard & MacFarlane, 1970; Camacho et al., 2000), which did not cover the entire island. Our new map has been obtained from a better distribution, resolution and accuracy of the land gravity data and with marine gravity data to better define the offshore structures. A new model of the sources of the gravity field

(low and high-density structures), reaching depths of approximately 20,000 m, has been obtained by applying our inversion method based on a genetic algorithm to the new gravity data set.

The gravity model exhibits a complex structure at depths shallower than ~7,000 m. Low-density structures found up to 4,000 m b.s.l. correspond to fractures, likely acting as feeder dikes of monogenetic volcanoes during the rejuvenated stage. The more significant deep high-density structures can be correlated with the intrusive bodies emplaced in the early formation of Gran Canaria and the magma plumbing system of the Miocene volcanic edifices. At the center of the island, gravity inversion results show structures associated with the syenitic core of the felsic central volcanic edifice.

The gravity inversion model made it possible to identify several zones of structural weakness, trending NW-SE, used for the magma to reach the surface in the Neocanaria area. Also, the model identifies a structural ENE-WSW lineament, which agrees with other recognized tectonic features of the archipelago. Indeed, the most important volcano-tectonic structure of Gran Canaria is the NW-SE Rift, which represents a long-lived rift zone that has controlled the volcanic activity at least since the Miocene. Besides, our results suggest that, after submarine growth mainly controlled in its NW sector by the ENE-WSW tectonic feature proposed by previous potential field data (Bosshard & MacFarlane, 1970; Blanco-Montenegro et al., 2018), the distribution of the main high-density bodies, as well as the growth of the central felsic complex associated with the Roque Nublo volcano, contributed to the present configuration of Gran Canaria Island.

Data Availability Statement

Land gravity data (gravity and anomalies values) presented as part of this study are provided as supplementary data available in the Zenodo repository (https://doi.org/10.5281/zenodo.6608699). Restrictions apply to the availability of the marine gravity data set, which were used under license for this study from third party.

Acknowledgments
Projects PID2019-104726GB-I00, CGL2015-63799-P and CGL2011-25494 of the Spanish Research Agency and funding for research groups of Complutense University of Madrid (UCM 2020 - GR29/20) have supported this research. We acknowledge Associate Editor Max Moorkamp, Michele Paulatto, and an anonymous reviewer for their constructive comments and suggestions which greatly improved our paper.

References

Amante, C., & Eakins, B. W. (2009). ETOPO1 1 arc-minute global relief model: Procedures, data sources and analysis. In *NOAA technical memorandum NESDIS NGDC-24*. National Geophysical Data Center, NOAA. https://doi.org/10.7289/V5C8276M

Anguita, F., & Hernán, F. (1975). A propagating fracture model versus a hot-spot origin for the Canary Islands. *Earth and Planetary Science Letters*, *27*(1), 11–19. https://doi.org/10.1016/0012-821X(75)90155-7

Anguita, F., & Hernán, F. (2000). The Canary Islands origin: A unifying model. *Journal of Volcanology and Geothermal Research*, *103*(1–4), 1–26. https://doi.org/10.1016/S0377-0273(00)00195-5

Araña, V., & Ortiz, R. (1991). The Canary Islands: Tectonics, magmatism and geodynamic framework. In A. B. Kampunzu & R. T. Lubala (Eds.), *Magmatism in extensional structural settings: The phanerozoic african plate* (pp. 209–224). Springer. https://doi.org/10.1007/978-3-642-73966-8-9

Arnoso, J., Benavent, M., Bos, M. S., Montesinos, F. G., & Vieira, R. (2011). Verifying the body tide at the Canary Islands using tidal gravimetry observations. *Journal of Geodynamics*, *51*(5), 358–365. https://doi.org/10.1016/j.jog.2010.10.004

Aulinas, M., Gimeno, D., Fernandez Turiel, J. L., Pérez-Torrado, F. J., Rodriguez-Gonzalez, A., & Gasperin, D. (2010). The Plio-quaternary magmatic feeding system beneath gran Canaria (Canary Islands, Spain): Constraints from thermobarometric studies. *Journal of the Geological Society of London*, *167*(4), 785–801. https://doi.org/10.1144/0016-76492009-184

Balcells, R., Barrera, J. L., Gómez, J. A., & Cueto, L. A. (1992). Mapa Geológico de España escala 1:100.000 1a edición (MAGNA). In *Hoja de la Isla de Gran Canaria (21-21/21-22)*. Instituto Tecnológico Geominero de España (ITGE). Serv. Pub. Ministerio de· Industria.

Balcells, R., Barrera, J. L., & Ruiz, M. T. (1990). Mapa geológico de España escala 1: 25.000, 1ª edición (MAGNA). In *Hoja de Arucas (1101-III-VI; 83-81; 83-82)* (p. 114). ITGE., Serv. Pub. Ministerio de Industria.

Banda, E., Dañobeitia, J. J., Suriñach, E., & Ansorge, J. (1981). Features of crustal structure under the Canary Islands. *Earth and Planetary Science Letters*, *55*(1), 11–24. https://doi.org/10.1016/0012-821X(81)90082-0

Barrera, J. L., & García Moral, R. (2011). *Mapa geológico de Canaria. Memorial general* (p. 502). GRAFCAN Ed.

Barton, J. (1986). The relationship between seismic velocity and density in the continental crust a useful constraint? *Geophysical Journal of the Royal Astronomical Society*, *87*(1), 195–208. https://doi.org/10.1111/j.1365-246X.1986.tb04553.x

Blanco-Montenegro, I., Montesinos, F. G., & Arnoso, J. (2018). Aeromagnetic anomalies reveal the link between magmatism and tectonics during the early formation of the Canary Islands. *Scientific Reports*, *8*(1), 42. https://doi.org/10.1038/s41598-017-18813-w

Blanco-Montenegro, I., Torta, J. M., García, A., & Araña, V. (2003). Analysis and modelling of the aeromagnetic anomalies of gran Canaria (canary islands). *Earth and Planetary Science Letters*, *206*(3–4), 601–616. https://doi.org/10.1016/S0012-821X(02)01129-9

Bosshard, E., & MacFarlane, D. J. (1970). Crustal structure of the Western Canary Islands from seismic refraction and gravity data. *Journal of Geophysical Research*, *75*(26), 4901–4918. https://doi.org/10.1029/jb075i026p04901

Bourcart, J., & Jeremine, E. (1937). La Grande Canarie. *Bulletin Volcanologique*, *2*(1), 3–77. https://doi.org/10.1007/bf03028397

Camacho, A. G., Montesinos, F. G., & Vieira, R. (2000). Gravity inversion by means of growing bodies. *Geophysics*, *65*(1), 95–101. https://doi.org/10.1190/1.1444729

Carracedo, J. C. (1999). Growths, structure, instability and collapse of Canarian volcanoes and comparisons with Hawaiian volcanoes. *Journal of Volcanology and Geothermal Research*, *94*(1–4), 1–19. https://doi.org/10.1016/S0377-0273(99)00095-5

Carracedo, J. C., Pérez-Torrado, F. J., Ancochea, E., Meco, J., Hernán, F., Cubas, C. R., et al. (2002). Cenozoic volcanism: II. The canary islands. In F. A. W. Gibbons & T. Moreno (Eds.), *The geology of Spain* (pp. 439–472). Geological Society of London. https://doi.org/10.1144/GOSPP.18

Collier, J. S., & Watts, A. B. (2001). Lithospheric response to volcanic loading by the canary islands: Constrains from seismic reflection data in their flexural moat. *Geophysical Journal International*, *147*(3), 660–676. https://doi.org/10.1046/j.0956-540x.2001.01506.x

Fedi, M., Cella, F., D'Antonio, M., Florio, G., Paoletti, V., & Morra, V. (2018). Gravity modeling finds a large magma body in the deep crust below the Gulf of Naples. *Italy. Sci Rep*, *8*(1), 8229. https://doi.org/10.1038/s41598-018-26346-z

Folger, D. W., McCullough, J. R., Irwin, B. J., Dodd, J. E., Strahle, W. J., Polloni, C. F., & Bouse, R. M. (1990). *Map showing free-air gravity anomalies around the Canary Islands, Spain, Miscellaneous Field Studies Map, MF-2098-B, p. (1 sheet)*. U.S. Geol. Surv.

Funck, T., Dickmann, T., Rihm, R., Krastel, S., Lykke, H., Andersen, T., & Schmincke, H. U. (1996). Reflection on seismic investigations in the volcaniclastic apron of Gran Canaria and implications for its volcanic evolution. *Geophysics Journal of Intelligence*, *125*(2), 519–536. https://doi.org/10.1111/j.1365-246X.1996.tb00015.x

Funck, T., & Schmincke, H. U. (1998). Growth and destruction of Gran Canaria deduced from seismic reflection and bathymetric data. *Journal of Geophysical Research*, *103*(B7), 15393–15407. https://doi.org/10.1029/98jb00388

García-Martínez, C., Rodriguez, F. J., & Lozano, M. (2018). Genetic algorithms. In R. Martí, P. Pardalos, & M. Resende (Eds.), *Handbook of heuristics 1–2* (pp. 431–464). https://doi.org/10.1007/978-3-319-07124-4_28

González de Vallejo, L., Hijazo Ramiro, T., & Ferrer Gijón, M. (2008). Engineering geological properties of the volcanic rocks and soils of the Canary Islands. *Soils & rocks*, *31*(1), 3–13. https://doi.org/10.28927/sr.311003

Guillou, H., Torrado, F. J. P., Machin, A. R. H., Carracedo, J. C., & Gimeno, D. (2004). The Plio-Quaternary volcanic evolution of Gran Canaria based on new K-Ar ages and magneto stratigraphy. *Journal of Volcanology and Geothermal Research*, *135*(3), 221–246. https://doi.org/10.1016/j.jvolgeores.2004.03.003

Hansen, A. (2009). Volcanología y geomorfología de la etapa de rejuvenecimiento plio-pleistocena de Gran Canaria (Islas Canarias). *Ph.D, Thesis, Universidad de Las Palmas de Gran canaria*, 400.

Hoernle, K., & Schmincke, H. U. (1993). The role of partial melting in the 15-ma geochemical evolution of gran canaria: A blob model for the canary hotspot. *Journal of Petrology*, *34*(3), 599–626. https://doi.org/10.1093/petrology/34.3.599

Jensen, M. (2016). Magma storage of the alkaline Tejeda cone sheet swarm, gran canaria, Spain. In *Examensarbete vid institutionen för geovetenskaper 362, degree Project published at department of Earth sciences* (p. 138). Uppsala University.

Karátson, D., Yepes, J., Favalli, M., Rodríguez-Peces, M. J., & Fornaciai, A. (2016). Reconstructing eroded paleovolcanoes on Gran Canaria, Canary Islands, using advanced geomorphometry. *Geomorphology*, *253*, 123–134. https://doi.org/10.1016/j.geomorph.2015.10.004

Krastel, S., & Schmincke, H. U. (2002). Crustal structure of northern Gran Canaria, Canary Islands, deduced from active seismic tomography. *Journal of Volcanology and Geothermal Research*, *115*(1–2), 153–177. https://doi.org/10.1016/S0377-0273(01)00313-4

Ledo, J., García-Merino, M., Larnier, H., Slezak, K., Piña-Varas, P., Marcuello, A., et al. (2021). 3D electrical resistivity of Gran Canaria island using magnetotelluric data. *Geothermics*, *89*, 101945. https://doi.org/10.1016/j.geothermics.2020.101945

Long, L. T., & Kaufmann, R. D. (2013). *Acquisition and Analysis of terrestrial gravity data*, Cambridge University Press, (p. 171).

Mangas, J., Pérez-Torrado, F. J., Gimeno, D., Hnasen, A., Paterne, M., & Guillou, H. (2002). Caracterización de los materiales volcánicos asociados a las erupciones holocenas de La Caldera de Pinos de Gáldar y edificios volcánicos adyacentes (Gran canaria). *Geogaceta*, *32*, 47–50.

Martínez-Arévalo, C., Mancilla, F., Helffrich, G., & Garcia, A. (2013). Seismic evidence of a regional sublithospheric low velocity layer beneath the Canary Islands. *Tectonophysics*, *608*, 586–599. https://doi.org/10.1016/j.tecto.2013.08.021

McDougall, I., & Schmincke, H. U. (1976). Geochronology of Gran Canaria, Canary Islands: Age of shield building volcanism and other magmatic phases. *Bulletin Volcanologique*, *40*(1), 57–77. https://doi.org/10.1007/BF02599829

Menéndez, I., Silva, P. G., Martín-Betancor, M., Pérez-Torrado, F. J., Guilloud, H., & Scaillet, S. (2008). Fluvial dissection, isostatic uplift, and geomorphological evolution of volcanic islands (Gran Canaria, Canary Islands, Spain). *Geomorphology*, *102*(1), 189–203. https://doi.org/10.1016/j.geomorph.2007.06.022

Michalewicz, Z. (1994). *Genetic algorithms + Data structures= Evolution programs* (2nd extended edition) (p. 340). Springer.

Montesinos, F. G., Arnoso, J., Benavent, M., & Vieira, R. (2006). The crustal structure of El Hierro (Canary Islands) from 3-d gravity inversion. *Journal of Volcanology and Geothermal Research*, *150*(1–3), 283–299. https://doi.org/10.1016/j.jvolgeores.2005.07.018

Montesinos, F. G., Arnoso, J., & Vieira, R. (2005). Using a genetic algorithm for 3-D inversion of gravity data in Fuerteventura (Canary Islands). *International Journal of Earth Sciences*, *94*(2), 301–316. https://doi.org/10.1007/s00531-005-0471-6

Montesinos, F. G., Arnoso, J., Vieira, R., & Benavent, M. (2011). Subsurface geometry and structural evolution of La Gomera Island based on gravity data. *Journal of Volcanology and Geothermal Research*, *199*(1–2), 105–117. https://doi.org/10.1016/j.jvolgeores.2010.10.007

Pérez-Torrado, F. J., Carracedo, J. C., & Mangas, J. (1995). Geochronology and stratigraphy of the Roque Nublo cycle (Gran Canaria, Canary Islands). *Journal of the Geological Society*, *152*(5), 807–818. https://doi.org/10.1144/gsjgs.152.5.0807

Rodriguez-Gonzalez, A. (2009). El vulcanismo Holoceno de Gran canaria. Aplicación de un sistema de información geográfico. *Ph.D. Thesis, Universidad de Las Palmas de Gran Canaria*, 423.

Rodriguez-Gonzalez, A., Fernandez-Turiel, J. L., Pérez-Torrado, F. J., Hansen, A., Aulinas, M., Carracedo, J. C., et al. (2009). The Holocene volcanic history of gran Canaria island: Implications for volcanic hazards. *Journal of Quaternary Science*, *24*(7), 697–709. https://doi.org/10.1002/jqs.1294

Rodriguez-Gonzalez, A., Fernandez-Turiel, J. L., Pérez-Torrado, F. J., Paris, R., Gimeno, D., Carracedo, J. C., & Aulinas, M. (2012). Factors controlling the morphology of monogenetic basaltic volcanoes: The Holocene volcanism of Gran Canaria (Canary Islands, Spain). *Geomorphology*, *136*(1), 31–44. https://doi.org/10.1016/j.geomorph.2011.08.023

Rodriguez-Gonzalez, A., Pérez-Torrado, F. J., Fernandez-Turiel, J. L., Aulinas, M., Paris, R., & Moreno-Medina, C. (2018). The Holocene volcanism of gran Canaria (Canary Islands, Spain). *Journal of Maps*, *14*(2), 620–629. https://doi.org/10.1080/17445647.2018.1526717

Rodríguez-Losada, J. A., Hernández-Gutiérrez, L. E., Olalla, C., Perucho, A., Serrano, A., & Eff-Darwich, A. (2009). Geomechanical parameters of intact rocks and rock masses from the Canary Islands: Implications on their flank stability. *Journal of Volcanology and Geothermal Research*, *182*(1–2), 67–75. https://doi.org/10.1016/j.jvolgeores.2009.01.032

Sainz-Maza Aparicio, S., Martí, J., Montesinos, F. G., Borreguero Gómez, A., Pereda de Pablo, J., Vaquero Fernández, P., & Calvo García-Maroto, M. (2019). Gravimetric study of the shallow basaltic plumbing system of Tenerife, Canary Islands. *Physics of the Earth and Planetary Interiors*, *297*, 106319. https://doi.org/10.1016/j.pepi.2019.106319

Schmincke, H. U. (1993). *Geological field guide of gran Canaria* (p. 227). Pluto Press. Retrieved from https://oceanrep.geomar.de/35737/

Schmincke, H. U., & Segschneider, B. (1998). Shallow submarine to emergent basaltic shield volcanism of gran canaria: Evidence from drilling into the volcanic apron (ODP leg 157). In P. P. E. Weaver, H. U. Schmincke, J. V. Firth, & W. Duffield (Eds.), *Proceedings of the ocean drilling program, scientific results 157* (pp. 141–181). Ocean Drilling Program. https://doi.org/10.2973/odp.proc.sr.157.110.1998

Schmincke, H. U., & Sumita, M. (1998). Volcanic evolution of gran canaria reconstructed from apron sediments: Synthesis of vicap project drilling. In P. P. E. Weaver, H. U. Schmincke, J. V. Firth, & W. Duffield (Eds.), *Proceedings of the Ocean drilling Program, scientific results* (Vol. *157*, pp. 443–469). https://doi.org/10.2973/odp.proc.sr.157.135.1998

Schmincke, H. U., Weaver, P. P. E., & Firth, J. V. (1995). Shipboard scientific party. *Proceedings of the ocean drilling program, initial reports, leg 157*, (Ocean Drilling Program), (p. 843). https://doi.org/10.2973/odp.proc.ir.157.1995

Spector, A., & Grant, F. S. (1970). Statistical methods for interpreting aeromagnetic data. *Geophysics*, *35*(2), 293–302. https://doi.org/10.1190/1.1440092

Syberg, F. J. R. (1972). A Fourier method for the regional-residual problem of potential fields. *Geophysical Prospecting*, *20*(1), 47–75. https://doi.org/10.1111/j.1365-2478.1972.tb00619.x

Troll, V., & Carracedo, J. C. (2016). *The geology of the Canary Islands*. Ed. Elsevier, (p. 636). https://doi.org/10.1016/B978-0-12-809663-5.00010-4

Troll, V. R., Walter, T. R., & Schmincke, H. U. (2002). Cyclic caldera collapse: Piston or piecemeal subsidence? Field and experimental evidence. *Geology*, *30*(2), 135–138. https://doi.org/10.1016/j.epsl.2006.09.042

Watts, A. B. (2000). The growth and decay of oceanic islands. In M. A. Summerfield (Ed.), *Geomorphology and global tectonics* (pp. 338–360). Wiley.

Ye, S., Canales, J. P., Rihm, R., Dañobeitia, J. J., & Gallart, J. (1999). A crustal transect trough the northern and northeastern part of the volcanic edifice of Gran Canaria, Canary Islands. *Journal of Geodynamics*, *28*(1), 3–26. https://doi.org/10.1016/S0264-3707(98)00028-3